

Kinetics of voiding and agglomeration of copper nanolayers on silica

R. Saxena,¹ M. J. Frederick,² G. Ramanath,^{2,*} W. N. Gill,¹ and J. L. Plawsky^{1,†}

¹Chemical Engineering Department, Rennselaer Polytechnic Institute, Troy, New York 12180, USA

²Department of Material Science and Engineering, Rennselaer Polytechnic Institute, Troy, New York 12180, USA

(Received 14 December 2004; revised manuscript received 27 June 2005; published 22 September 2005)

We report the kinetics of annealing-induced dewetting of sub-60-nm-thick Cu films on silicon dioxide based upon *in situ* electrical resistance, *ex situ* scanning electron microscopy and atomic force microscopy measurements. Cu films become discontinuous upon annealing between ~ 300 and 600°C through void nucleation and island formation. Films dewet via two kinetically limiting sequential processes: void nucleation by grain boundary grooving (activation energy $E_a=1.2$ eV) followed by void growth and islanding through surface diffusion of Cu at the Cu-SiO₂ interface, i.e., surface spreading, (activation energy $E_a=0.7$ eV). The kinetic pathway for dewetting is film-thickness dependent. For film thinner than 20 nm, complete dewetting occurs between 300 and 450°C and is limited by surface diffusion of Cu at the Cu-SiO₂ interface, while for thicker films (>20 nm) dewetting is governed solely by grain boundary grooving. This thickness-dependent dewetting is described by a phenomenological model validated by the evolution of mean roughness and lateral correlation length of the Cu surface. This work provides a framework for evaluating the morphological stability on ultrathin metal films on dielectric materials, in particular those being considered for use in micro- and nanodevice structures.

DOI: [10.1103/PhysRevB.72.115425](https://doi.org/10.1103/PhysRevB.72.115425)

PACS number(s): 61.72.Mm, 47.20.Hw, 61.72.Cc, 68.55.-a

I. INTRODUCTION

Understanding the morphological instabilities in metal films on various substrates is of both scientific and technological interest due to the entailing implications on the properties, reliability, and performance of micro- and nanodevices wired with metal films. In particular, understanding the conditions under which copper (Cu) films become discontinuous on dielectric materials¹ and devising strategies to suppress dewetting, are of great importance to realize next generation integrated circuits. In this paper, we report the thickness-dependent kinetics and atomistic mechanisms of dewetting of <60 -nm-thick Cu films on silicon dioxide (SiO₂) to serve as a benchmark to compare the stability of Cu films on different substrates.

Dewetting is generally initiated by heterogeneous void formation² during annealing, and is driven by excess energy due to high fraction of grain boundaries, interfaces and surfaces,^{3–7} or residual stresses.^{8,9} The atomistic mechanisms of dewetting and related phenomena have been addressed by modeling,^{2–10} and to a lesser extent, experimental measurements of Au and Ag film agglomeration kinetics during annealing.^{11–15} Most experimental data on thin film dewetting has been qualitative in nature, with limited insights on the kinetic mechanisms of void nucleation and void growth processes.

The earliest study of kinetics of metal dewetting was by Kane *et al.*,¹¹ by *in situ* resistance measurements coupled with *ex situ* scanning electron microscopy (SEM) to map the morphological changes in 6–8-nm-thick Au films encapsulated by graded layers of ZnS–CdS on glass substrates. Using a heuristic model, they calculated the activation energy of Au film breakup as $E_a=1.8$ eV, corresponding to Au lattice diffusion. Jiran and Thompson^{12,13} using *in situ* transmission electron microscopy (TEM) and *in situ* laser scatter-

ing film reflectivity measurements, obtained very different activation energies on 40–90-nm-thick Au films on SiO₂. They attributed $E_a=1.2$ eV for void nucleation, and $E_a=1.1$ – 1.9 eV for void growth. The activation energy variation was explained based on an empirical model where the void growth rate varied inversely with the cube of the film thickness (a^{-3}). This model yielded an effective activation energy $E_a=1.4$ eV, implying that Au surface diffusion on the Au-SiO₂ interface is the rate limiting mechanism. Due to lack of sufficient data, however, it was not possible to conclude if the thickness dependence of activation energy was real or constituted a change in the kinetic mechanism. Similar thickness-dependence has been observed in Ag films as well. Based on *ex situ* TEM observations of dewetting in 35–165 nm Ag films on silica, Presland *et al.*¹⁴ reported a cubic dependence of incubation time on film thickness. They obtained activation energies of 0.64 eV for void nucleation and 0.71 eV for void spreading in a 118-nm-thick film. Kim *et al.*¹⁵ used *in situ* resistance measurements and the cubic dependence of film thickness on incubation time determined by Presland *et al.* to obtain an activation energy of 0.32 eV for 35–70 nm Ag film dewetting on SiO₂. These values studies again are consistent with surface diffusion at the Ag-SiO₂ interface being the kinetically limiting mechanism for film dewetting, but the thickness dependence on activation energy was not investigated.

Although annealing can also induce grain growth,^{16,17} we expect that this phenomenon to be suppressed because the grain sizes in our films—verified by an independent study¹⁸—are roughly of the order of the film thickness. Grain growth suppression in films with grain size equal to or larger than the film thickness has been attributed to grain boundary grooving by Mullins.¹⁹ This prediction has been validated experimentally by recent measurements in 80-nm-thick Ag films on SiN (Ref. 20) revealing that grain growth is arrested

in the temperature regime where the film dewets from the substrate. At high temperatures, grain-boundary grooving induced dewetting is thought to be kinetically favored over grain growth due to the lower activation energy of 0.274 eV for grain growth, than that measured for film dewetting.^{14,15}

Recently, morphological instabilities in nm-thick films of Cu on different dielectric substrates have been studied.^{21–23} While these studies describe the importance of effects of substrate morphology and chemistry on Cu film dewetting, a quantitative measure of the kinetics and underlying atomistic mechanisms governing break up are yet to be determined. The modeling efforts have also suffered from a lack of experimental data on kinetics of film agglomeration. The only model comparison was shown by Wong *et al.*¹⁰ using the data of Jiran and Thompson^{12,13} which could not account for the entire spectrum of film thickness studied and was only able to predict a growth velocity 100 times less than that experimentally observed.

Here, we report the kinetics of dewetting of <60-nm-thick Cu films on SiO₂ and elucidate the effects of film thickness and annealing temperature on the dewetting pathway. We show that for films thinner than 20 nm, dewetting is limited by Cu surface spreading, i.e., surface diffusion at the Cu-dielectric interface ($E_a=0.7$ eV). For thicker films, dewetting is limited by diffusion of Cu at the grain boundaries ($E_a=1.2$ eV). We explain the thickness-dependent wetting behavior based upon a phenomenological model validated by the evolution of surface morphology quantified by parameters determined from atomic force microscopy measurements.

II. EXPERIMENTAL DETAILS

The substrates used in this study were RCA-cleaned 3-in.-diameter Si wafers, with a 1- μ m-thick SiO₂ cap layer deposited by plasma-enhanced chemical vapor deposition (PECVD) in an Applied Materials Plasmatherm® tool. Cu films with thicknesses between 15 to 60 nm were then grown on SiO₂ by using a CVC® dc magnetron sputter system pumped to a base vacuum of 5×10^{-7} Torr. Sputtering was done in presence of argon at 5 mTorr pressure and 2.3 kW power applied at the Cu electrode. The film deposition rate at these conditions was around 950–1000 Å/min. Due to the relatively short time for film deposition (<1 min), the temperature rise during sputtering is considered negligible and the substrates were effectively at room temperature (27 °C).¹⁸ No external cooling was applied. The thicknesses of the oxide and Cu films were determined using ellipsometry and Rutherford backscattering spectrometry (RBS), respectively. Samples were transported from the deposition chamber in an air-tight container to minimize Cu oxidation for all further measurements. Some effect of Cu oxide formed during transportation on the ensuing measurements cannot be discounted. Film sheet resistance (R_S) was measured *in situ* during annealing from room temperature to 700 °C at predetermined ramp rates of 1–10 °C/min and temperatures T , in a computer-interfaced vacuum furnace (base pressure 1×10^{-8} Torr) equipped with a four point probe in the van der Pauw configuration. The sheet resistance

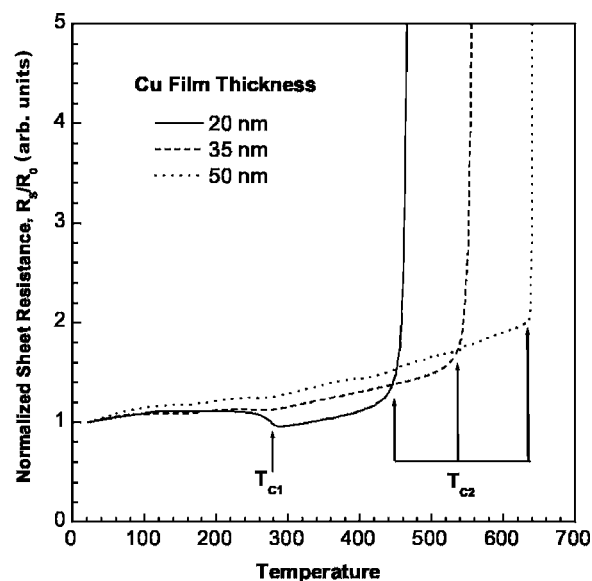


FIG. 1. Representative curves depicting the *in situ* sheet resistance behavior of 15–60-nm-thick Cu films during vacuum annealing at 6 °C/min. Sheet resistance, R_S is normalized to the room temperature value R_0 .

R_S was measured by placing the probes in a van der Pauw configuration. This technique does not require high symmetry placement of the probes on the sample, and is sensitive only to changes occurring in the film, and is insensitive to local changes, e.g., near the probe due to small changes in position due to drift or reaction.^{24,25} In order to directly correlate these measurements with the Cu film morphology, we annealed selected samples in vacuum (base pressure 8×10^{-7} Torr) on a custom designed stage to different temperatures and observed the morphological changes in a JEOL JSM 6332 SEM after cooling to room temperature. There was no film deposited on top of the annealed samples prior to the SEM imaging as this would have masked some of the morphological characteristics. Some sample charging effects are visible on completely dewetted samples. A Park Scientific Auto-probe CP® AFM tool was used to quantitatively characterize the film roughness of the samples from both annealing experiments.

III. RESULTS AND DISCUSSION

A. *In situ* sheet resistance

Figure 1 shows the normalized sheet-resistance-temperature (R_S - T) signatures obtained from Cu films of different thicknesses annealed at 6 °C/min. All the films show an initial linear increase in R_S between 25 and 250 °C due to increased electron-phonon scattering reflected in the temperature coefficient of resistance. This R_S increase is reversible upon cooling. For films with thickness ≤ 20 nm the R_S drops irreversibly by $\sim 20\%$ between 250–300 °C at a characteristic temperature T_{C1} , which is a function of annealing rate. The R_S decrease is reproducible at different annealing rates and only occurs for thinner films, indicating that it is not an artifact. Upon further annealing, R_S increases sharply

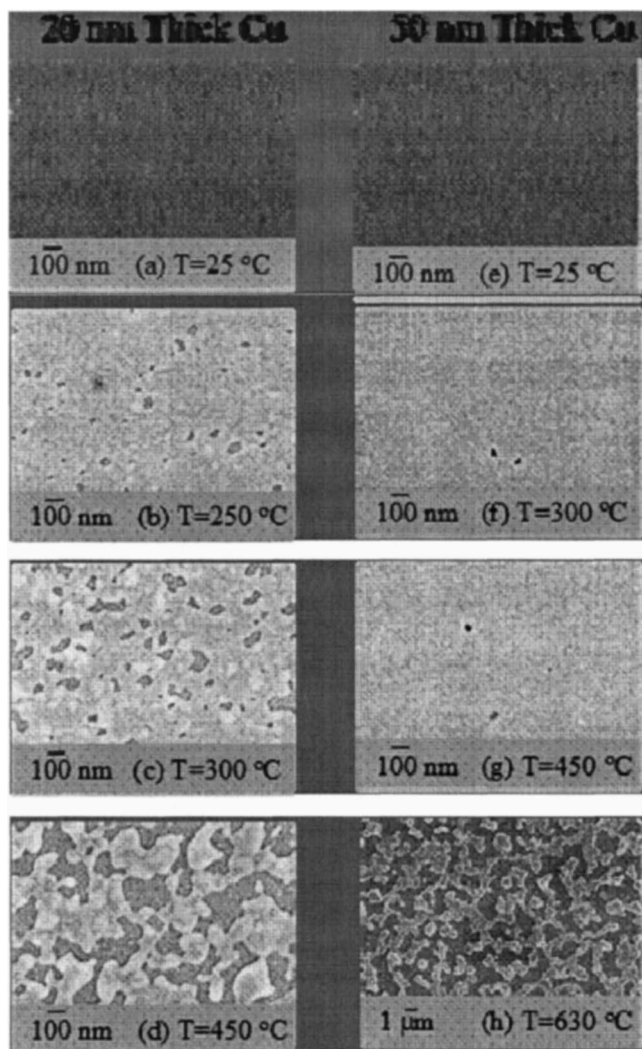


FIG. 2. Representative SEM micrographs depicting the morphological changes in 20 and 50 nm thick Cu films. The images were captured from samples annealed to the indicated temperatures, and cooled to room temperature.

by about a factor of 100 at a characteristic temperature T_{C2} which ranges between 450 and 650 °C, depending upon annealing rate and film thickness. Films thicker than 20 nm do not exhibit the R_S drop, but show the abrupt R_S increase at T_{C2} after the reversible linear R_S - T behavior.

B. Film morphology

Figure 2 shows the SEM micrographs obtained from samples annealed to temperatures corresponding to different portions of the R_S - T curves. The bright-contrast regions represent the metallic Cu film due to enhanced scattering of the electrons, while the regions with dark contrast in the micrographs represent lower lying areas, with the darkest regions representing the exposed substrate surface. The edge of the Cu islands represent a slightly brighter contrast which is due to sample charging by electrons of the SEM beam. The electrons accumulate at the edge of the conductive Cu film as there are no conducting pathways available through the ex-

posed nonconducting SiO_2 substrate. Films thinner than 20 nm show void formation at T_{C1} , characterized by the appearance of small regions of the underlying substrate [Fig. 2(b)].

One possible explanation of the observed R_S drop in this temperature regime could be an effective increase in the film cross-sectional area due to the material removed from the grain boundary grooves being deposited back in the film at the top surface. The film at this moment is still connected and the electrons can find effective pathways through a thicker effective cross-section of the film. This effective local cross-sectional area increase is possible only in thinner films because the voids are smaller and the film can remain connected. This kind of decrease has been observed experimentally earlier although no explanation was offered.²⁶ A more detailed investigation is required to further understand the 3D morphological changes in the film just prior to dewetting. Upon annealing to T_{C2} the voids grow, leading to *complete Cu film dewetting* by island formation [Figs. 2(c) and 2(d)]. The abrupt increase in R_S at this temperature is thus due to the decrease in the effective conduction path length.

For thicker films, the voids form islands at T_{C2} , with no observable intermediate stages of void nucleation or growth [Figs. 2(e)–2(h)]. The final value of R_S after film break-up is ~ 3 –4 orders magnitude higher than that of as-deposited film, and corresponds to film dewetting by islanding. The dewetting temperatures of the thicker films are higher than that measured for the thinner ones, consistent with previous reports.¹⁵

C. Kinetics

The T_{Ci} and the characteristic times τ corresponding to a typical thermally activated kinetic process can be described by the Arrhenius expression given by

$$\tau = A \exp\left(\frac{E_a}{kT_{Ci}}\right), \quad (1)$$

where, A is a proportionality constant and is a function of the film-substrate combination, k is the Boltzmann constant, and E_a is the activation energy. We apply this expression to τ - T_{Ci} combinations at different annealing rates, obtained experimentally for each film thickness. The characteristic time, τ refers to the time corresponding to T_{Ci} for each annealing rate. Fitting our experimental data for a Cu film thickness of 20 nm, we obtain activation energies of 1.2 ± 0.1 eV and 0.7 ± 0.1 eV for processes corresponding to T_{C1} and T_{C2} , respectively (see Fig. 3). Identical activation energy values are obtained by applying a modified Kissinger analysis (Appendix), which is a more common approach in evaluating the activation energy using R_S - T signatures.^{25,27,28} The activation energy values of 1.2 eV and 0.7 eV correspond to previously reported values for diffusion of Cu at grain boundaries and Cu- SiO_2 interface, respectively.²⁹ In the context of electrical resistance measurements and SEM observations, our kinetics results indicate that Cu films thinner than 20 nm dewet by a two-step process of grain boundary grooving followed by spreading on the Cu- SiO_2 interface. Complete dewetting as determined by the sheet resistance increase is controlled by

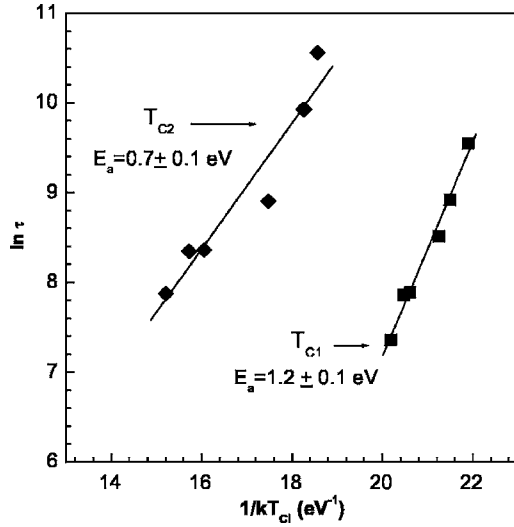


FIG. 3. Arrhenius plots for thermally activated processes characterized by temperatures T_{C1} and T_{C2} . The characteristic times τ were obtained for different ramp rates between 0.5 and 10 °C/min for a 20-nm-thick Cu film on SiO_2 . The temperature readings have an average error of ± 10 °C. (The corresponding error on the x -axis is about $0.1\text{--}0.2\text{ eV}^{-1}$ which makes plotting error bars difficult.)

the surface diffusion of Cu atoms on the film-substrate interface and this is the rate limiting step.

In order to verify the validity of our kinetics analysis for dewetting of films thicker than 20 nm, we used the Mullins model² that relates grain boundary grooving kinetics to film thickness a , annealing temperature T_{Ci} , room-temperature grain boundary diffusivity of the metal D_o , activation energy for void formation E_a , Boltzmann constant k , angle at the film surface-groove root θ_i , film surface energy γ_i , film atomic volume Ω , and the number of atoms per unit area in the film n_i , and is given by

$$\tau = \left(\frac{a}{0.973 \tan(\theta_i)} \right)^4 \frac{kT_{Ci}}{D_o \gamma_i \Omega^2 n_i} \exp\left(\frac{E_a}{kT_{Ci}}\right). \quad (2)$$

Since the variation in the linear kT term is negligible compared to the exponential term and the other terms in the pre-exponent are nearly constant in the temperature range of our interest, for a given film thickness the above reduces to a modified Arrhenius relationship given by

$$\tau = Ba^4 \exp\left(\frac{E_a}{kT_{Ci}}\right). \quad (3)$$

This expression enables the efficient determination of the activation energy for a wide range of film thicknesses using a minimal number of experiments if grain boundary grooving is the mechanism of film dewetting. Mullins only considered the temperature dependence of diffusivity, D , which gives rise to the temperature dependent exponential term and constant D_o .² The other parameters like γ and Ω were considered constant, which is also true for our temperature range of interest. Fitting T_{C2} , a , and τ data experimentally determined for films of varying thickness >20 nm into Eq. (3), we obtain $E_a = 1.2 \pm 0.1$ eV. This value is in good agreement with

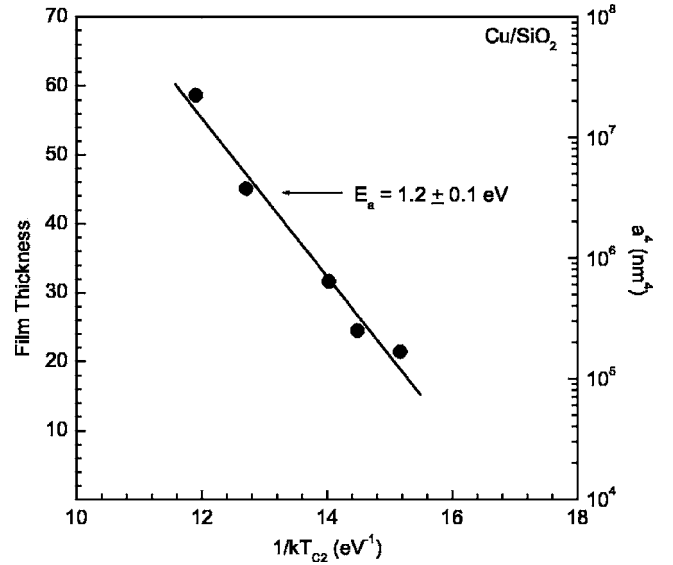


FIG. 4. Plot using the modified Mullins model [Eq. (3)] to determine the activation energy of the thermally activated process characterized by T_{C2} , measured for films with different thicknesses at the annealing rate of 6 °C/min. The temperature readings have an average error of ± 10 °C.

that of Cu grain boundary grooving (Fig. 4), and indicates that the Mullins model for grain grooving is a good description of the dewetting of Cu films with thicknesses ≥ 20 nm on silica substrates. Thus, for thicker films, grain boundary grooving is the rate limiting step controlling complete island formation or agglomeration.

D. Atomistic mechanisms

Based on our results, we propose a phenomenological model to describe the atomistic mechanisms of dewetting of

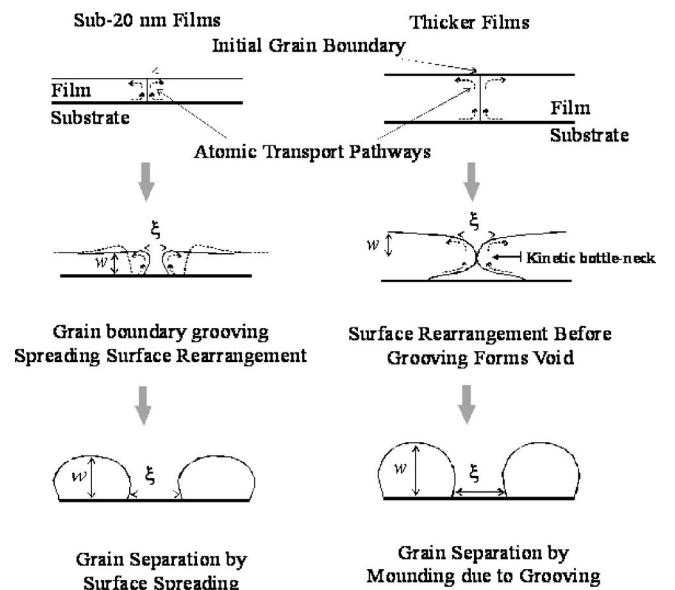


FIG. 5. Phenomenological model describing film dewetting by void formation and islanding for thin and thick films.

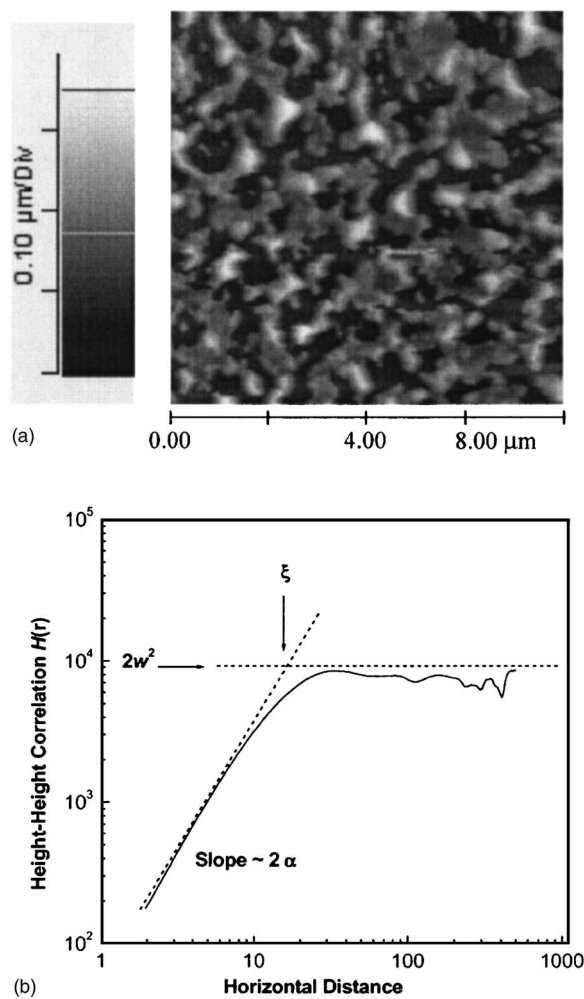


FIG. 6. (a) A representative AFM image of a 50-nm-thick Cu film annealed to 630 °C. The dark regions represent the voids and the white contrast regions represent the mounds. (b) Height-height correlation function obtained from (a). The different surface roughness parameters are indicated.

Cu films on SiO₂. The key features of the model are illustrated schematically in Fig. 5. For films thinner than ~20 nm, film dewetting occurs in two stages. Voids nucleate at grain boundaries by Cu atom diffusion at the grain boundaries. Since the film thickness is small, the grooves rapidly extend to the Cu-silica interface after which the intergranular voids grow via Cu atom transport on the silica surface (spreading), leading to complete dewetting. In thicker films, however, grain boundary grooving being the slowest (highest activation energy) step limits the void formation. Surface spreading of Cu atoms at the Cu-SiO₂ interface occurs simultaneously as the grains groove, but by the time the grooves initiate a void at the Cu-SiO₂ interface and the film surface merge and span the film thickness, the lateral spatial extents of the voids are already large, and separate Cu islands are formed (Fig. 5). In particular, Cu transport through the ungrooved portions of the grain boundaries (see schematic sketch in Fig. 5) constitute the kinetic bottleneck and hence grain boundary diffusion is the kinetic rate limiting process that governs complete dewetting.

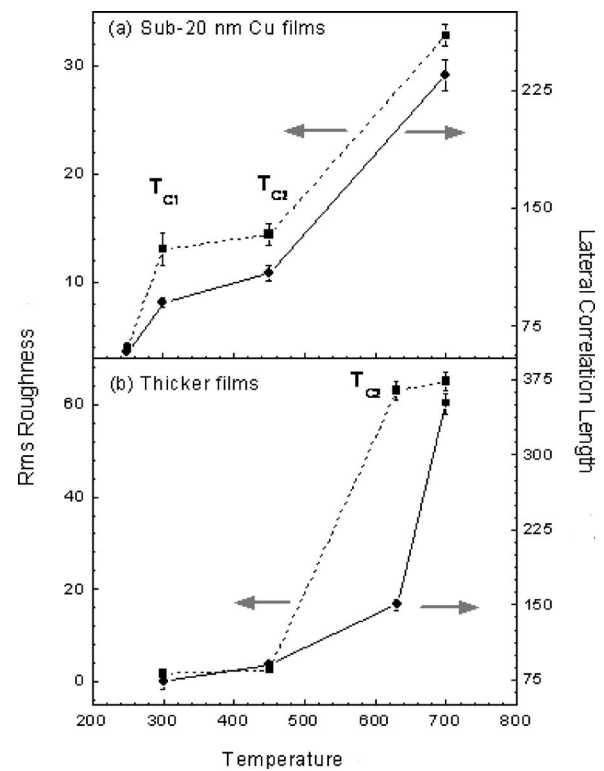


FIG. 7. Evolution of root-mean-square roughness and lateral correlation length plotted as a function of annealing temperature for (a) 20-nm-thick and (b) 50-nm-thick Cu films.

This model is verified by contact-mode AFM analysis of changes in rms roughness w , and lateral correlation length ξ , determined using the height-height correlation function $H(\mathbf{r})$ which provides a *quantitative* average measure of the surface morphology. $H(\mathbf{r})$ is given by $\langle [h(\mathbf{r}) - h(0)]^2 \rangle$, where $h(\mathbf{r})$ is the surface height at position \mathbf{r} , relative to the mean surface height $h(0)$, and $\langle \dots \rangle$ denotes statistical average. A sample AFM image and the corresponding height-height correlation plot are shown in Fig. 6. The scaling hypothesis for a self-affine random surface³⁰ requires $H(\mathbf{r}) = \rho^2 r^{2\alpha}$ for $r \ll \xi$ and $H(\mathbf{r}) = 2w^2$ for $r \gg \xi$, where ρ is the average local slope, and α is the microscale roughness exponent.³¹ The average peak to valley distance is given by w , which physically means the depth of the void or height of an island formed depending upon the stage of agglomeration, and is of the order of film thickness. The correlation length, ξ , defines a representative lateral dimension of a rough surface. If the distance between two surface points is within ξ , the heights of these two points can be considered correlated, else they are independent of each other. Generally, the separation between islands (void size) can be found for mounded surfaces using a 2D correlation function. The island size is a function of system correlation length, ζ (which determines randomness of islands) and average void size λ . For the limiting case of $\zeta/\lambda \ll 1$ (i.e., random surfaces) in 2D, the slope of the height-height correlation function is approximated by w^2/λ^2 . Thus, for our surfaces, which are essentially random over the scan length (5 μm), a 1D correlation function can be used. The slope in 1D is $2w^2/\xi$, where ξ is the lateral correlation length. In reality, ξ is a function of both system correlation length, ζ

and average mound separation λ and but for the limiting case it is directly related to the void size. Thus, a measure of ξ would give the average size of a void, or spacing between the islands depending upon the stage of agglomeration.

The parameters extracted by this approach are plotted as a function of annealing temperature in Fig. 7. For films thinner than 20 nm, both w and ξ increase near T_{C1} , due to void nucleation and propagation along grain boundaries to the Cu-silica interface. The depth of the void (w) is of the order of film thickness, while the size of the void is reflected by ξ . Subsequently, between T_{C1} and T_{C2} , ξ increases while w remains essentially constant, indicating void growth primarily by in-plane spreading of the newly formed mounds on the surface. Around T_{C2} both w and ξ increase, indicating island formation due to void pinching and this continues much beyond T_{C2} . For films thicker than 20 nm, both w and ξ increase together only around $T_{C2} \sim 630^\circ\text{C}$ indicating that complete dewetting occurs in a single-step by mound formation via grain boundary grooving. Beyond T_{C2} , both w and ξ are almost constant indicating that the islands formed are no longer spreading, unlike the case for thinner films. Thus, the phenomenological model proposed to explain the two rate limiting steps of grain boundary grooving and surface spreading governing dewetting in thick and thin films respectively is confirmed by AFM measurements.

The existence of different rate limiting steps, grain boundary grooving and surface spreading, dependent on film thickness, are shown in this work for the first time. This has important implications, especially in the microelectronics industry where ultrathin metal films are employed, as suppressing the surface diffusion pathway on the film-substrate interface to prevent agglomeration can be achieved by substrate surface modification.^{32,33}

IV. SUMMARY

Sub-60-nm Cu films on silica dewet by two different pathways depending upon the film thickness. Films thinner than 20 nm dewet in two kinetically limiting sequential steps: void nucleation by grain-boundary diffusion (activation energy $E_a = 1.2$ eV) followed by void growth and islanding by Cu surface spreading ($E_a = 0.7$ eV). For thinner films, the latter step of void growth by surface spreading is the rate controlling step because the grooves rapidly extend to the Cu-silica interface after which the intergranular voids grow via Cu atom transport on the silica surface, leading to islanding. In thicker films dewetting is limited by grain boundary grooving ($E_a = 1.2$ eV). By the time the grooves initiated at the film surface and the Cu-silica interface merge and span the film thickness, the lateral spatial extents of the voids is already large, and separate Cu islands are already formed. The effect of grain growth leading to a possible increase in grain sizes prior to the dewetting process requires a more detailed investigation and is not considered in the present work. Thus, in addition to the well-known grain boundary grooving mechanism, surface diffusion of Cu at the Cu-SiO₂ interface can serve as an additional dewetting pathway if the grooving process occurs across a short length-scale,

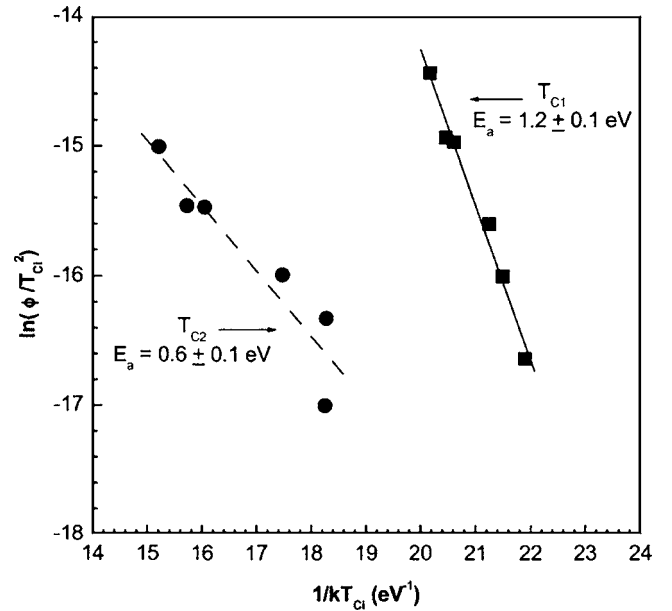


FIG. 8. Activation energy determination using the Kissinger analysis for a 20-nm-thick Cu film annealed at different ramp rates.

i.e., in thinner films. An important consequence is that dewetting can be suppressed in ultrathin films if surface diffusion at the film-substrate interface is curtailed, e.g., by enhancing the bonding interactions at the interface via substrate surface modification^{32,33} and processing. Hence, these findings would be of particular interest to the microelectronics industry where ultrathin Cu films will be used for device wiring.

ACKNOWLEDGMENTS

The authors gratefully acknowledge funding support from the Center for Advanced Interconnect Science and Technology, Semiconductor Research Corporation Contract No. 2002-MC-995, New York State, GR's NSF CAREER Grant No. DMR 9984478 and Professor Bergmann Award from the U.S.-Israel Binational Science Foundation.

APPENDIX

The measurement of electrical resistance can be used to determine kinetics of thin film phase changes by adapting the Kissinger equation usually applied on differential thermal analysis data,¹⁵⁻¹⁷

$$\ln\left(\frac{\phi}{T_{Ci}^2}\right) = -\frac{E_a}{kT_{Ci}},$$

where $\phi = dT/dt$ is the ramp rate in $^\circ\text{C/s}$ and T_{Ci} is the critical temperature. In order to determine the activation energies of the kinetic processes from resistivity measurements, we identified the critical temperatures T_{C1} and T_{C2} for different ϕ (see Fig. 8) for 20 nm Cu films. These yield activation energies of 1.2 ± 0.1 eV and 0.6 ± 0.1 eV, corresponding to Cu grain boundary grooving and surface diffusion, respectively.

*Electronic address: ramanath@rpi.edu

†Electronic address: plawsky@rpi.edu

- ¹M.-A. Nicolet, *Thin Solid Films* **52**, 415 (1978).
- ²W. W. Mullins, *J. Appl. Phys.* **28**, 333 (1957).
- ³D. J. Srolovitz and S. A. Safran, *J. Appl. Phys.* **60**, 247 (1986).
- ⁴D. J. Srolovitz and S. A. Safran, *J. Appl. Phys.* **60**, 255 (1986).
- ⁵K. T. Miller, F. F. Lange, and D. B. Marshall, *J. Mater. Res.* **5**, 151 (1990).
- ⁶T. P. Nolan and R. Sinclair, *J. Appl. Phys.* **71**, 720 (1992).
- ⁷D. J. Srolovitz and M. G. Goldiner, *J. Test. Eval.* **47**, 31 (1995).
- ⁸F. Y. Genin, W. W. Mullins, and P. Wynblatt, *Acta Metall. Mater.* **41**, 3541 (1993).
- ⁹D. J. Srolovitz, W. Yang, and M. G. Goldiner, *J. Mater.* **403**, 3 (1996).
- ¹⁰H. Wong, P. W. Voorhees, M. J. Miksis, and S. H. Davis, *Acta Mater.* **48**, 1719 (2000).
- ¹¹W. M. Kane, J. P. Spratt, and L. W. Hershinger, *J. Appl. Phys.* **37**, 2085 (1966).
- ¹²E. Jiran and C. V. Thompson, *J. Electron. Mater.* **19**, 1153 (1990).
- ¹³E. Jiran and C. V. Thompson, *Thin Solid Films* **208**, 23 (1992).
- ¹⁴A. E. Presland, G. L. Price, and D. L. Trimm, *Prog. Surf. Sci.* **3**, 63 (1973).
- ¹⁵H. C. Kim, T. L. Alford, and D. R. Allee, *Appl. Phys. Lett.* **81**, 4287 (2002).
- ¹⁶C. V. Thompson, *Annu. Rev. Mater. Sci.* **30**, 159 (2000).
- ¹⁷P. Damman, N. Baudet, and G. Reiter, *Phys. Rev. Lett.* **91**, 216101 (2003).
- ¹⁸E. V. Barnat, D. Nagakura, P.-I. Wang, and T.-M. Lu, *J. Appl. Phys.* **91**(3), 1667 (2002).
- ¹⁹W. W. Mullins, *Acta Metall.* **6**, 414 (1958).
- ²⁰R. Dannenberg, E. A. Stach, J. R. Groza, and B. J. Dresser, *Thin Solid Films* **370**, 54 (2000).
- ²¹J.-Y. Kwon, T.-S. Yoon, K.-B. Kim, and S.-H. Min, *J. Appl. Phys.* **93**(6), 3270 (2003).
- ²²T. L. Alford, L. Chen, and K. S. Gadre, *Thin Solid Films* **429**, 248 (2003).
- ²³R. Saxena, O. Rodriguez, W. Cho, W. N. Gill, and J. L. Plawsky, *J. Non-Cryst. Solids* **350**, 14 (2004).
- ²⁴L. J. van der Pauw, *Philips Res. Rep.* **13**, 1 (1958).
- ²⁵M. J. Frederick and G. Ramanath, *J. Appl. Phys.* **95**(1), 363 (2004).
- ²⁶*Handbook of Thin Film Technology*, edited by Leon I. Maissel and Reinhard Glang (McGraw-Hill, New York, 1970), Vol. 1.
- ²⁷H. E. Kissinger, *J. Res. Natl. Bur. Stand.* **57**(4), 217 (1956).
- ²⁸C. Detavernier, S. Rossnagel, C. Noyan, S. Guha, C. Cabral Jr., and C. Lavoie, *J. Appl. Phys.* **94**(5), 2874 (2003).
- ²⁹D. A. Porter and K. E. Easterling, *Phase Transformations in Metals and Alloys*, 2nd ed. (Chapman and Hall, London, 1992).
- ³⁰Y. P. Zhao, G. C. Wang, and T.-M. Lu, *Characterization of Amorphous and Crystalline Roughness—Principles and Applications* (Academic, New York, 2001).
- ³¹The microroughness parameter, α , is not plotted as it is not a relevant parameter in our conceptual model.
- ³²P. G. Ganesan, A. P. Singh, and G. Ramanath, *Appl. Phys. Lett.* **85**(4), 579 (2004).
- ³³G. Ramanath, G. Cui, M. Stukowski, X. Guo, P. G. Ganesan, A. V. Ellis, K. Vijayamohan, P. Doppelt, and M. Lane, *Appl. Phys. Lett.* **83**(2), 383 (2003).